Received: 1 May 2023 | Revised: 20 March 2025 | Accepted: 23 March 2025

DOI: 10.1002/esp.70055

RESEARCH ARTICLE

ESPL WILEY

The susceptibility of subglacial carbonates to frost weathering

Matej Lipar[1] | Matija Zorn[1] | Mateja Ferk[1] | Klemen Cof[2] | Janko Čretnik[3]

[1]Anton Melik Geographical Institute, Research Centre of the Slovenian Academy of Sciences and Arts, Ljubljana, Slovenia

[2]Department of Geography, University of Ljubljana, Ljubljana, Slovenia

[3]Slovenian National Building and Civil Engineering Institute, Ljubljana, Slovenia

Correspondence
Matej Lipar, Anton Melik Geographical Institute, Research Centre of the Slovenian Academy of Sciences and Arts, Ljubljana, Slovenia.
Email: matej.lipar@zrc-sazu.si

Funding information
The Slovenian Research and Innovation Agency, Grant/Award Numbers: J6-3141, P6-0101, I0-0031

Abstract

The retreat of glaciers over the last century exposed subglacial carbonate, which formed between the glacier ice body and bedrock due to regelation. As such they have implications for paleoenvironmental studies. They are particularly significant as indicators of past glacial presence – since they can form under glacial conditions – and recent glacial retreat, given their high susceptibility to rapid weathering. However, their susceptibility to frost weathering remains relatively unexplored. This study investigates the susceptibility of subglacial carbonates to frost weathering by exposing them to freeze–thaw cycles in a freezing tank. The study demonstrates that subglacial carbonates are inherently weak and prone to weathering, with around a quarter of the samples experiencing breakage into shreds. While exact rates of weathering in natural settings remain challenging to determine, the laboratory conditions provided a framework for evaluating the fundamental response of subglacial carbonates to temperature stresses.

KEYWORDS
Alps, cryogenic weathering, frost action, glaciokarst, Mt. Kanin, Mt. Triglav, rock decay, subglacial carbonate

1 | INTRODUCTION

Geology and geomorphology are both representations of intricate Earth system dynamics and processes, and can consequently be used to reconstruct palaeoenvironment (Widdowson, 1997), which includes biotic parameters like fossil assemblage, and abiotic parameters like climate. An intriguing example of this multidisciplinary combination is the glaciers' erosional potential to polish the rocks on a small scale (Benn & Evans, 2010; Siman-Tov et al., 2017) and carve glacier cirques and valleys on a larger scale (White, 1970). Glaciers are important for palaeoenvironmental research, either through the study of their growth or retreat (Ivy-Ochs et al., 2008; Kerschner & Ivy-Ochs, 2008; Palacios et al., 2022), the study of their ice (Higgins et al., 2015; O'Brien et al., 1995) or the study of their deposits, e.g., the deposition of till (Hart & Boulton, 1991) and precipitation of the coating layer by accreting material to the abraded surface (Siman-Tov et al., 2017) or subglacial carbonates due to regelation (Figure 1) (Hallet, 1976). The retreat of glaciers over the last century exposed many surfaces with these subglacial carbonate deposits (Lipar et al., 2021), resulting in the interest of their potential to contribute to the overall understanding of the palaeoenvironment.

Subglacial carbonates are relatively thin carbonate crusts (Figures 1 and 2) formed between the ice and bedrock by regelation at the glacier base on the lee side of a bedrock protuberance (Hallet, 1976; Lemmens, Lorrain, & Haren, 1982; Ng & Hallet, 2002; Souchez & Lemmens, 1985). Mineralogically they mostly consist of calcite characterised by elongated columnar crystals growing perpendicularly or inclined to the bedrock (Figure 6a), or by layered structures of micrite and/or microsparite (Hallet, 1976; Lipar et al., 2021; Rabassa & Coronato, 2023). Minor amounts of aragonite, dolomite and various amounts of detrital minerals may also be present (Ford, Fuller, & Drake, 1970; Lipar et al., 2021; Rabassa & Coronato, 2023). Subglacial carbonates occur globally and have been reported from Antarctica (Aharon, 1988; Frisia et al., 2017; Hellstrom et al., 2008), Europe (Colucci, 2016; Gabrovec et al., 2014; Lacelle, 2007; Lemmens, Lorrain, & Haren, 1982; Sharp, Tison, & Fierens, 1990; Souchez & Lemmens, 1985; Thomazo et al., 2017), North America (Ford, Fuller, & Drake, 1970; Hallet, 1976; Refsnider et al., 2012; Sharpe & Shaw, 1989), South America (Rabassa, 2010; Rabassa & Coronato, 2023), Asia (Risheng et al., 2003) and Oceania (Peterson & Moresby, 1979).

Their palaeoenvironmental importance has long been established, especially because uranium/thorium (U/Th) dating brought the

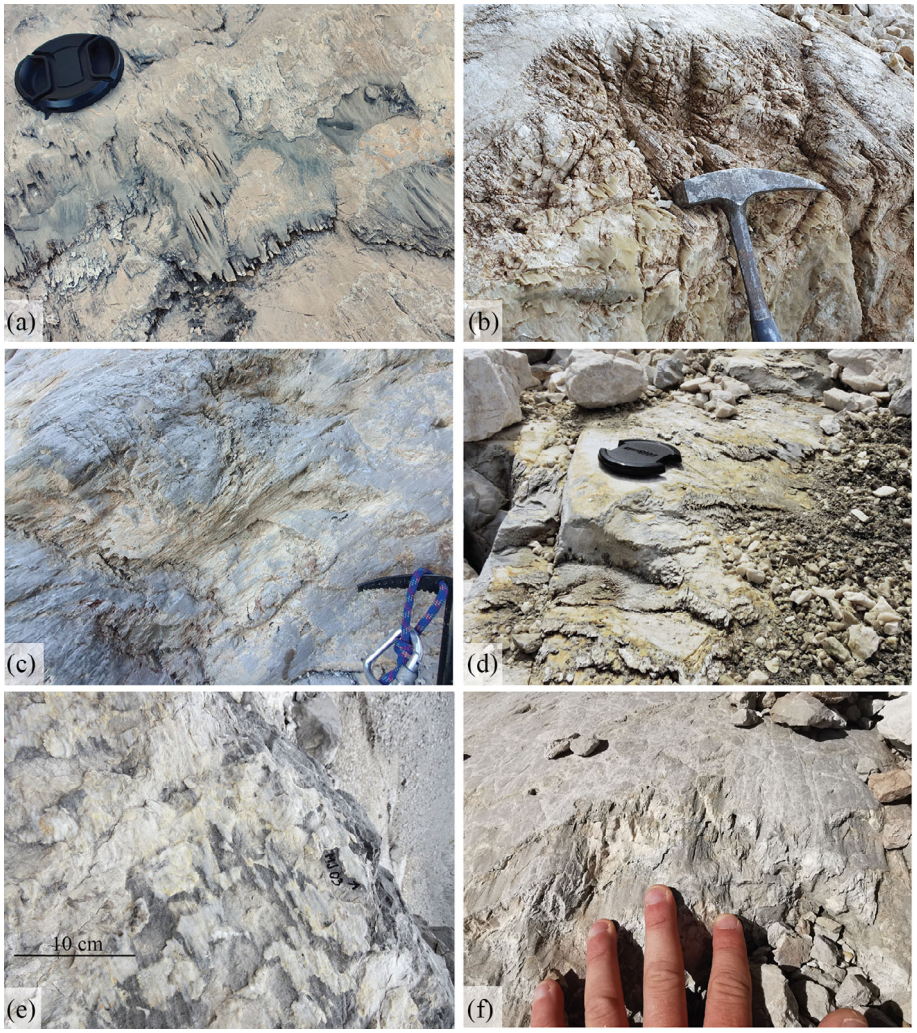

FIGURE 1 The occurrence of subglacial carbonates near the Triglav Glacier, Slovenia (a), near Debeli Namet Glacier, Montenegro (b), near Skuta Glacier, Slovenia (c), near Kanin Glacier, Italy (d), from Prokletije Mountains, Albania (e) and on Monte Civetta, Italy (f). Photo courtesy for (f) of Jure Tičar.

precision of the exact timing of their precipitation and consequently palaeoenvironmental interpretation into the reliable chronological context (Hellstrom et al., 2008; Lipar et al., 2021; Refsnider et al., 2012; Sharp, Tison, & Fierens, 1990; Souchez & Lemmens, 1985; Thomazo et al., 2017). In general, the time span of the formation of subglacial carbonate deposits is tied to glacial activity, which, over time scales may range from years to centuries and include hiatuses, depending on environmental conditions and meltwater dynamics. Mostly, the ages of the samples have been provided as a single bulk age for the sample (Lipar et al., 2021; Refsnider et al., 2012), but the interval between 29.5 and 17.0ka from the sample from Antarctica (Hellstrom et al., 2008) provides an example of continuous or continual growth for more than 12 thousand years.

Furthermore, their exposure to atmospheric processes after the retreat of overlying glacier ice has equally been recognised as an important factor, because they have been characterised as features prone to frost weathering (Ford, Fuller, & Drake, 1970) and therefore a possible key to determine the constant presence of the glaciers since the formation of subglacial carbonates, and/or elucidate glaciers' recent Holocene retreat (Lipar et al., 2021). Indeed, freeze–thaw cycles significantly impact the physical and mechanical properties of rocks, primarily due to non-uniform thermal stresses within the solid matrix and the phase transitions of pore water (Qi et al., 2023b). Nevertheless, the susceptibility of subglacial carbonates to frost weathering has merely relied on the observation that they mostly tend to appear in recently deglaciated areas and that their occurrence away from the glaciers relatively quickly diminishes (Ford, Fuller, & Drake, 1970; Gabrovec et al., 2014). This paper investigates whether subglacial carbonates are inherently susceptible to frost weathering, as has been suggested by prior studies but not empirically tested. Additionally, the study explores how these processes can be extrapolated over time to better understand their role as indicators of past glacial presence.

2 | MATERIALS AND METHODS

2.1 | Study area

Subglacial carbonates were sampled at the edge of the retreating Kanin Glacier (~30% of analysed samples) and Triglav Glacier (~70% of the analysed samples), located in the western Julian Alps in Italy and the central Julian Alps in Slovenia (southeastern Alps) (Figure 2).

The Kanin Glacier is located on a massif mostly composed of Main Dolomite overlain by Dachstein Limestone, both Upper Triassic. The latter is well karstified and reshaped by Pleistocene glacial processes (Kunaver, 1983), so the massif has a typical high mountain glaciokarst topography with a high density of deep caves (Securo, Del Gobbo, & Colucci, 2022; Telbisz, Mari, & Szabó, 2011). During the Pleistocene glacial periods, an ice cap covered most of

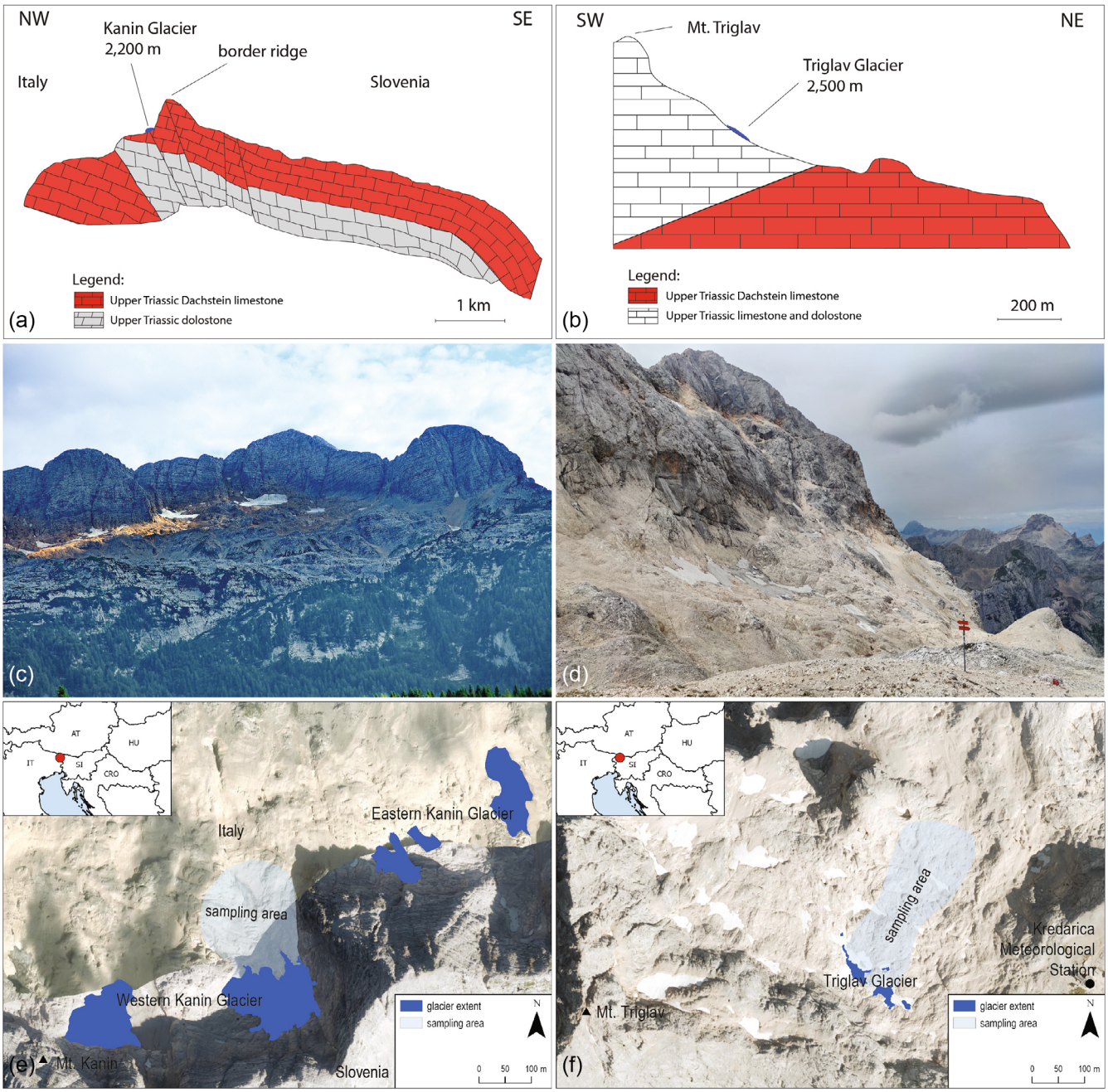

FIGURE 2 (a,c) The location of the ice mass remnants of the Kanin Glacier with geological cross-section, remodified from Antonini & Squassino (1992) and Audra (2000) (a), and the view from the northwest (c). (b,d) The location of the ice mass remnants of the Triglav Glacier with geological cross-section, remodified from Lipar et al. (2024) (b), and the view from the southeast (d). The current ice patches of the Kanin (e) and Triglav (f) glaciers with the sampling areas.

the massif with just the highest peaks and main ridges exposed above it (Ferk et al., 2017; Telbisz, Mari, & Szabó, 2011), whilst at present only small ice patches remained. They are located north of the main Kanin ridge (on the Italian side) with their main elevation around 2,200m a.s.l.: Eastern Kanin Glacier (*It*. Ghiacciaio orientale del Canin) and Western Kanin Glacier (*It*. Ghiacciaio occidentale del Canin) (Ferk et al., 2017; Triglav Čekada, Zorn, & Colucci, 2014) with a total area (measured in 2012) of 0.12 km^2 (Securo, Del Gobbo, & Colucci, 2022).

The Triglav Glacier is located on a massif composed of Upper Triassic limestone and dolomite (Pleničar, Ogorelec, & Novak, 2009; Ramovš, 2000). During the Pleistocene glacial periods, an ice cap covered also most of this massif. Since the end of the Little Ice Age (mid-19th century), the Triglav Glacier retreated from ca. 0.46 km^2 to less than 0.005 km^2 with its approximate elevation of 2,500m a.s.l. (Lipar et al., 2021). The presently exposed glaciokarst environment contains a range of features including caves, karren, polished surfaces and moraines (Lipar et al., 2021; Tičar et al., 2018; Tóth & Veress, 2019).

The Julian Alps are among the wettest in the Alps (Ogrin et al., 2023); at Kanin, the mean annual precipitation is >3,300mm and the mean annual air temperature is around 1°C at 2,203 m a.s.l. (Colucci, 2016; Colucci et al., 2014; Securo et al., 2022; Securo, Del Gobbo, & Colucci, 2022), whilst at Triglav the mean annual precipitation is >2000mm and the mean annual air temperature around −0.7°C at 2,514 m a.s.l. (Slovenian Environment Agency, 2024).

2.2 | Laboratory analyses

The sampling of subglacial carbonate fragments was conducted using flat screwdrivers and a geological hammer and then transported to the Laboratory for Stone, Aggregates and Recycled Materials of the Slovenian National Building and Civil Engineering Institute for frost resistance analysis.

The frost resistance of the samples was determined by a mass loss test comprising 56 freeze–thaw cycles in air and water using Kambič freezing tank (model IWB-150 CCK) (Prick, 2004a). The procedure was conducted according to standard SIST EN 12371:2010, however, the sample sizes are excluded from this standard as slabs of rock (i.e., subglacial carbonate) in the required size are not existent. Instead, we used 39 samples of subglacial carbonates from the field site which include their naturally occurring sizes when they break off from the bedrock (~1 to 5 g mass) as well as larger artificially broken fragments from the bedrock (up to 13 g mass). An additional eight samples of limestone (i.e., surrounding bedrock) with subglacial carbonate cemented on them were tested through the same 56 cycles to verify the preferable detachment of subglacial carbonates from the host rock during frost weathering.

Before and after the freeze–thaw cycles, the samples were dried in a ventilated oven at a temperature of (70°C ± 5°C) until they reached the constant mass before their mass was recorded. This is assumed to have been attained when the difference between two weighings at an interval of (24 h ± 2 h) is not greater than 0.1% of the first of these two masses. The weight scale used was the Mettler weight scale, model PC 2000, with a precision of 0.01 g. Its measurement uncertainty is ±0.008 g at 1 g and ±0.017 g at 500 g. Then, the samples were soaked in water for 48 hours. Subsequently, prior to being placed in the freezing tank, they were weighed in air and in water. The same procedure is repeated after the completion of 56 freeze–thaw cycles.

For freeze–thaw procedure, the samples were individually placed in aluminium cups with holes on the bottom; this is to prevent the floating of the cups when water runs into the freezing tank as well as to allow the water to run off the cups for a dry freeze–thaw cycle. The cups with samples were then placed in the freezing tank with an automatic control system to programme the freeze–thaw cycles within the chamber with a tolerance of ± 2°C. The samples were placed in the tank and positioned at least 10 mm apart from each other, and at least 20 mm away from the tank sides. The reference sample containing the temperature measuring device was placed in the middle of the samples to be tested.

Each cycle consisted of a 6 h freezing period in the air (dry conditions), followed by a 6 h thawing period during which the samples are immersed in water. A cycle starts at a temperature between +5°C and +20°C. In the next 2 h samples are cooled to a temperature between 0°C and −8°C and in the next 4 h samples are cooled to a temperature between −8°C and −12°C. After that the samples are within 30 minutes totally immersed in water and in the next 2.5 h temperature rises to between +5°C and +20°C and stays there for the next 3 h. The whole cycle lasts approximately 12 h and repeats 56 times (Figure 3).

2.3 | Meteorological data and freeze–thaw scenarios

The data from the Kredarica Meteorological Station (2,514 m a.s.l.; Figure 2f) (obtained from the Slovenian Environment Agency), which is only 400 m away from the Triglav Glacier, spans from 1955 to 2021

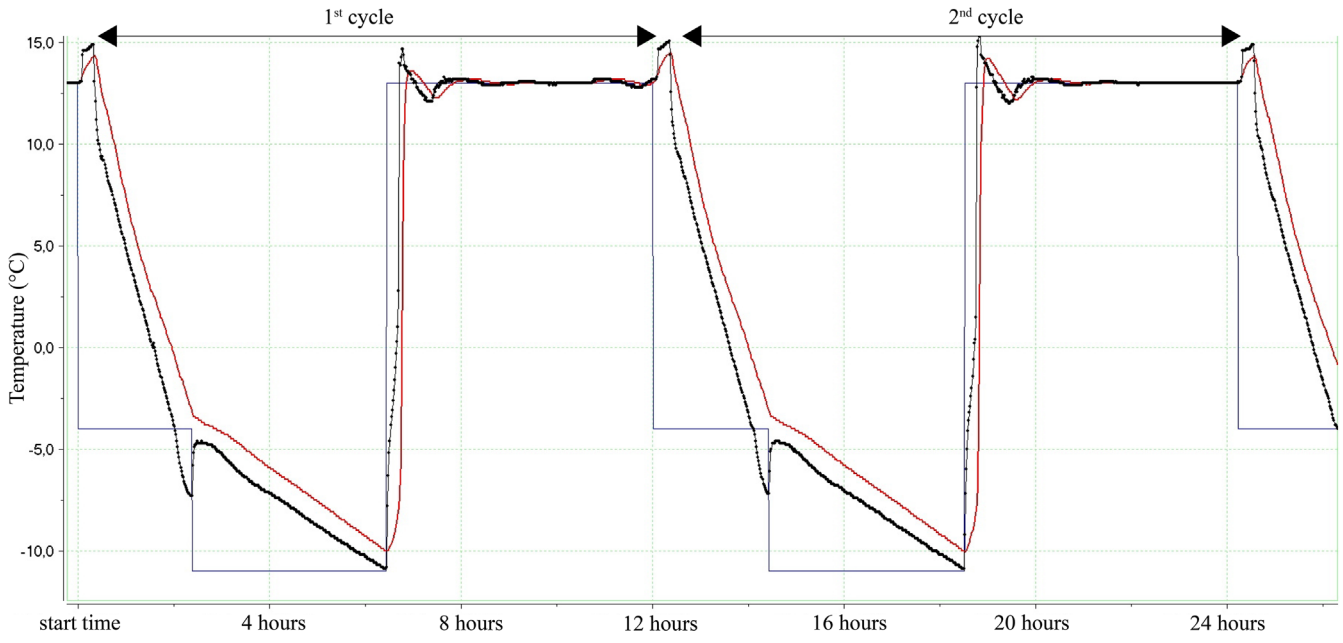

FIGURE 3 A section of the freezing tank's log, illustrating two freeze–thaw cycles with all temperature conditions (in °C). The blue line represents the set temperature regime. This is the ideal line in accordance with the instructions of the standard. The red line represents the temperature variation within the material. For this study, due to the small size of the samples, we used one limestone prism (a piece measuring 50 × 50 × 300 mm), into which a sensor was inserted. The black dotted line represents the air temperature in the tank chamber.

(i.e., 67 years) and includes daily temperature measurements at 7:00, 14:00 and 21:00 (local time, GMT + 1) and the total amount of snow cover on that day. These data were used for constructing realistic freeze–thaw scenarios for the region for timely extrapolation of freeze–thaw cycles.

We provide nine different scenarios of freeze–thaw cycles (Table 1): a scenario where 0°C represents the theoretical freezing point (cycle = > 0°C | ≤ 0°C | > 0°C), a scenario where only temperatures below 0°C are considered to cause freezing (cycle = > 0°C | < 0°C| > 0°C) and a scenario where only temperatures below −3°C are considered (cycle = > 0°C| < −3°C| > 0°C). All scenarios are then additionally considered only when the snow cover is less than 40 cm thick, and also when there is no snow cover. The reasoning for different scenarios is discussed in Section 4.1.

A Python script was used to calculate the total number of freeze–thaw cycles in the region of Kredarica Meteorological Station: for any given temperature data point, its value was multiplied by the next data point. A negative or zero (0) result indicates a temperature change past the freezing threshold. In the case of 0°C temperature values (for scenarios 1, 4 and 7) the first previous non-zero temperature data point is used instead. Different values are attributed to each temperature change depending on whether the temperature fell below or rose above the freezing point. A cycle of frost weathering is then defined as a negative change (indicating freezing) followed by a positive change (indicating thawing).

3 | RESULTS

3.1 | Loss of mass

Fifty-six freeze–thaw cycles showed variable loss of mass of the subglacial carbonate samples (Table 2), which can be classified into four different groups for a clear presentation.

One of the samples had undetectable change (i.e., 0.00 g) in mass before and after freeze–thaw cycles. This sample is considered an outlier, as no rock type is completely resistant to freeze–thaw weathering (Park, Hyun, & Park, 2014; Ruedrich, Kirchner, & Siegesmund, 2010; Zhang et al., 2023); however, the absence of detectable mass loss, in this case, could likely be attributed to the limits of the weighing system's sensitivity or uncertainties, which may have been insufficient to capture minimal changes in mass.

TABLE 1 Calculation scenarios of freeze–thaw cycles.

Scenarios	Scenario type
Scenario 1	>0 °C| ≤ 0°C| > 0°C, snow cover
Scenario 2	>0 °C| < 0°C| > 0°C, snow cover
Scenario 3	>0 °C| < −3°C| > 0°C, snow cover
Scenario 4	>0°C| ≤ 0°C| > 0°C, snow cover less than 40 cm
Scenario 5	>0°C| < 0°C| > 0°C, snow cover less than 40 cm
Scenario 6	>0 °C| < −3°C| > 0°C, snow cover less than 40 cm
Scenario 7	>0°C| ≤ 0°C| > 0°C, no snow cover
Scenario 8	>0°C| < 0°C| > 0°C, no snow cover
Scenario 9	>0°C| < −3°C| > 0°C, no snow cover

Amongst the 39 subglacial carbonate samples tested, 9 samples broke down into larger or almost equally sized shreds. This represents 23% of the analysed samples. The breakage is defined here where the cumulative broken shreds exceeded 10% of mass loss, partially following the definition of breakage by Schubert (2002) where the largest broken shred needs to exceed 10% of mass loss.

Twenty-nine samples (74% of all pure subglacial carbonates) experienced loss of mass lower than 10%. On average, the loss of mass was 2.62% (Figure 4a,b).

Small broken fragments were detected on six out of eight samples with subglacial carbonate crusts still cemented on the limestone (broken fragments were detached subglacial carbonates), reflecting that in 75% of cases, partial detachment occurs when run through fifty-six freeze–thaw cycles.

3.2 | Loss of apparent volume

The loss of apparent volume can only be calculated for the 29 samples (74% of all pure subglacial carbonates) which experienced loss of mass lower than 10%. The original apparent (weight) volume was calculated by subtracting the original water mass from the original air mass; similarly, the final apparent volume after freeze–thaw cycles was obtained by subtracting water final mass from air final mass of the samples. On average, the loss of apparent volume was 2.58% (Figure 4e), which, in turn, shows the negative volumetric strain (i.e., a change in volume of a rock specimen) on average −0.026.

3.3 | Correlations between mass, apparent volume and density and their changes

The correlation coefficient between the original mass of the samples and the percentage of mass lost (which ranges from 0% to 7.57% with a standard deviation of 2.47) is 0.082, suggesting a very weak positive relationship. This indicates that the original mass (i.e., from 1.15 g to 13.19 g within our study; Figure 4c) has almost no predictive capacity for the extent of mass loss during frost weathering. Even when samples with breakage are included (this ranges from 1.05 g to 13.38 g), the relationship remains statistically insignificant, implying that the physical size of the sample does not inherently determine its susceptibility to mass loss under frost weathering conditions.

The relationship between the percentage of mass lost and the original density of the samples (Figure 4d) yields a correlation coefficient of −0.047, reflecting a negligible and statistically insignificant negative association. This weak correlation indicates that – variations in the original density of the samples (which ranges from 2.39 to 2.70 g/cm^3) do not significantly impact the proportion of mass lost during the weathering process.

For samples that did not experience breakage, the correlation between the percentage of lost volume and the percentage of lost mass is extremely strong, with a coefficient of 0.954. This near-linear relationship implies a consistent proportionality between mass and volume loss for intact samples (Figure 4f). For instance, a sample losing 5% of its mass is likely to exhibit an equivalent percentage of volume loss, provided no structural collapse occurs.

TABLE 2 Basic sample characteristics before and after freeze–thaw cycles. Note that M_2 (dry to a constant mass) cannot be greater than M_{s0} (saturated with water and weighed in air). M_{h0} (weighed in water), however, is always smaller than M_2. In one of the measurements, it is highly likely that, with such a delicate sample weighing 2.36 g, a small particle detached during handling, which could explain the illogical difference in masses between M_2 and M_{s0}.

Sample IDA = Triglav glacierB = Kanin glacier	Material	Dry mass 1 (g) M_1	Dry mass 2 (g) M_2	Original mass (g) M_{s0}	Water mass (g) M_{h0}	Weight volume (g) V_{b0}	Density (g/cm^3)	Final mass (g) M_{s56}	Water final mass (g) M_{h56}	Weight volume (g) V_{b56}	Lost mass (g)	Lost mass (%)	Lost weight volume (g)	Lost volume (%)	Final density (g/cm^3)	Density difference (g/cm^3)
29B	Subg. carb.	2.36	2.36	2.11	1.24	0.87	2.42529	2.11	1.24	0.87	0.00	0.00	0.00	0.00	2.42529	0.00000
13A	Subg. carb.	10.85	10.85	11.17	6.71	4.46	2.50448	11.15	6.69	4.46	0.02	0.18	0.00	0.00	2.50000	−0.00448
9A	Subg. carb.	2.81	2.81	2.89	1.7	1.19	2.42857	2.88	1.69	1.19	0.01	0.35	0.00	0.00	2.42017	−0.00840
27A	Subg. carb.	7.32	7.32	7.5	4.55	2.95	2.54237	7.47	4.52	2.95	0.03	0.40	0.00	0.00	2.53220	−0.01017
24A	Subg. carb.	9.3	9.3	9.56	5.64	3.92	2.43878	9.52	5.61	3.91	0.04	0.42	0.01	0.26	2.43478	−0.00399
10A	Subg. carb.	4.54	4.54	4.71	2.76	1.95	2.41538	4.69	2.74	1.95	0.02	0.42	0.00	0.00	2.40513	−0.01026
8A	Subg. carb.	2.21	2.21	2.29	1.35	0.94	2.43617	2.28	1.34	0.94	0.01	0.44	0.00	0.00	2.42553	−0.01064
30A	Subg. carb.	8.5	8.5	8.69	5.27	3.42	2.54094	8.65	5.25	3.40	0.04	0.46	0.02	0.58	2.54412	0.00318
20A	Subg. carb.	1.89	1.89	1.92	1.19	0.73	2.63014	1.91	1.18	0.73	0.01	0.52	0.00	0.00	2.61644	−0.01370
16A	Subg. carb.	5.31	5.31	5.48	3.35	2.13	2.57277	5.43	3.3	2.13	0.05	0.91	0.00	0.00	2.54930	−0.02347
18B	Subg. carb.	2.09	2.09	2.18	1.30	0.88	2.47727	2.16	1.29	0.87	0.02	0.92	0.01	1.14	2.48276	0.00549
26A	Subg. carb.	3.66	3.66	3.65	2.3	1.35	2.70370	3.61	2.27	1.34	0.04	1.10	0.01	0.74	2.69403	−0.00967
22B	Subg. carb.	10.07	10.07	10.40	6.32	4.08	2.54902	10.28	6.26	4.02	0.12	1.15	0.06	1.47	2.55721	0.00819
26B	Subg. carb.	3.14	3.14	3.34	2.00	1.34	2.49254	3.29	1.97	1.32	0.05	1.50	0.02	1.49	2.49242	−0.00011
28B	Subg. carb.	1.98	1.98	2.49	1.53	0.96	2.59375	2.45	1.50	0.95	0.04	1.61	0.01	1.04	2.57895	−0.01480
30B	Subg. carb.	1.76	1.76	1.83	1.13	0.70	2.61429	1.80	1.11	0.69	0.03	1.64	0.01	1.43	2.60870	−0.00559
25A	Subg. carb.	9.21	9.21	9.23	5.74	3.49	2.64470	9.06	5.66	3.40	0.17	1.84	0.09	2.58	2.66471	0.02001
15A	Subg. carb.	5.24	5.24	5.37	3.26	2.11	2.54502	5.27	3.18	2.09	0.1	1.86	0.02	0.95	2.52153	−0.02349
9B	Subg. carb.	1.31	1.31	1.41	0.82	0.59	2.38983	1.38	0.81	0.57	0.03	2.13	0.02	3.39	2.42105	0.03122
2A	Subg. carb.	7.92	7.92	8.27	4.93	3.34	2.47605	8.05	4.79	3.26	0.22	2.66	0.08	2.40	2.46933	−0.00672
12A	Subg. carb.	6.15	6.15	6.39	3.81	2.58	2.47674	6.17	3.67	2.50	0.22	3.44	0.08	3.10	2.46800	−0.00874
25B	Subg. carb.	1.09	1.09	1.15	0.69	0.46	2.50000	1.11	0.67	0.44	0.04	3.48	0.02	4.35	2.52273	0.02273
28A	Subg. carb.	3.78	3.78	3.87	2.36	1.51	2.56291	3.73	2.28	1.45	0.14	3.62	0.06	3.97	2.57241	0.00950
14A	Subg. carb.	3.4	3.4	3.48	2.18	1.30	2.67692	3.35	2.07	1.28	0.13	3.74	0.02	1.54	2.61719	−0.05974
21A	Subg. carb.	4.54	4.54	4.58	2.85	1.73	2.64740	4.33	2.71	1.62	0.25	5.46	0.11	6.36	2.67284	0.02544
22A	Subg. carb.	10.53	10.53	10.75	6.51	4.24	2.53538	10.12	6.16	3.96	0.63	5.86	0.28	6.60	2.55556	0.02018
1A	Subg. carb.	12.59	12.59	13.19	7.79	5.40	2.44259	12.23	7.2	5.03	0.96	7.28	0.37	6.85	2.43141	−0.01118
29A	Subg. carb.	6.55	6.55	6.7	4.1	2.60	2.57692	6.2	3.81	2.39	0.5	7.46	0.21	8.08	2.59414	0.01722
4A	Subg. carb.	3.39	3.39	3.58	2.14	1.44	2.48611	3.31	1.96	1.35	0.27	7.54	0.09	6.25	2.45185	−0.03426

TABLE 2 (Continued)

Sample IDA = Triglav glacierB = Kanin glacier	Material	Dry mass 1 (g) M_1	Dry mass 2 (g) M_2	Original mass (g) M_{s0}	Water mass (g) M_{h0}	Weight volume (g) V_{b0}	Density (g/cm^3)	Final mass (g) M_{s56}	Water final mass (g) M_{h56}	Weight volume (g) V_{b56}	Lost mass (g)	Lost mass (%)	Lost weight volume (g)	Lost volume (%)	Final density (g/cm^3)	Density difference (g/cm^3)
5A	Subg. carb.	1.75	1.75	1.85	1.08	0.77	2.40260	1.71	1.02	0.69	0.14	7.57	0.08	10.39	2.47826	0.07566
23A	Subg. carb.	4.69	4.69	4.81	2.89	1.92	2.50521	-	-	-	-	-*	-	-	-	-
19B	Subg. carb.	1.24	1.24	1.32	0.78	0.54	2.44444	-	-	-	-	-*	-	-	-	-
3A	Subg. carb.	1.99	1.99	2.11	1.25	0.86	2.45349	-	-	-	-	-*	-	-	-	-
6A	Subg. carb.	12.71	12.71	13.38	7.82	5.56	2.40647	-	-	-	-	-*	-	-	-	-
7A	Subg. carb.	1.08	1.08	1.1	0.65	0.45	2.44444	-	-	-	-	-*	-	-	-	-
11A	Subg. carb.	2.53	2.53	2.6	1.56	1.04	2.50000	-	-	-	-	-*	-	-	-	-
17A	Subg. carb.	2.85	2.85	2.99	1.79	1.20	2.49167	-	-	-	-	-*	-	-	-	-
18A	Subg. carb.	0.99	0.99	1.05	0.64	0.41	2.56098	-	-	-	-	-*	-	-	-	-
19A	Subg. carb.	4.83	4.83	4.94	3.03	1.91	2.58639	-	-	-	-	-*	-	-	-	-
1B	Subg. carb. on Lstn	53.49	53.46	-	-	-	-	-	-	-	-	-**	-	-	-	-
13B	Subg. carb. on Lstn	4.99	4.99	-	-	-	-	-	-	-	-	-**	-	-	-	-
21B	Subg. carb. on Lstn	58.35	58.31	-	-	-	-	-	-	-	-	-**	-	-	-	-
15B	Subg. carb. on Lstn	26.01	25.99	-	-	-	-	-	-	-	-	-**	-	-	-	-
31A	Subg. carb. on Lstn	632.19	-##	-	-	-	-	-	-	-	-	-**	-	-	-	-
32A	Subg. carb. on Lstn	487.8	-##	-	-	-	-	-	-	-	-	-**	-	-	-	-
20B	Subg. carb. on Lstn	48.61	48.57	-	-	-	-	-	-	-	-	-***	-	-	-	-
23B	Subg. carb. on Lstn	3.71	3.71	-	-	-	-	-	-	-	-	-***	-	-	-	-

*Sample breakage; i.e., loss of mass greater than 10%.
**Detectable breakage of subglacial carbonates from limestone.
***Undetectable breakage of subglacial carbonates from limestone.
##Sample weighed on a different scale due to a larger mass.

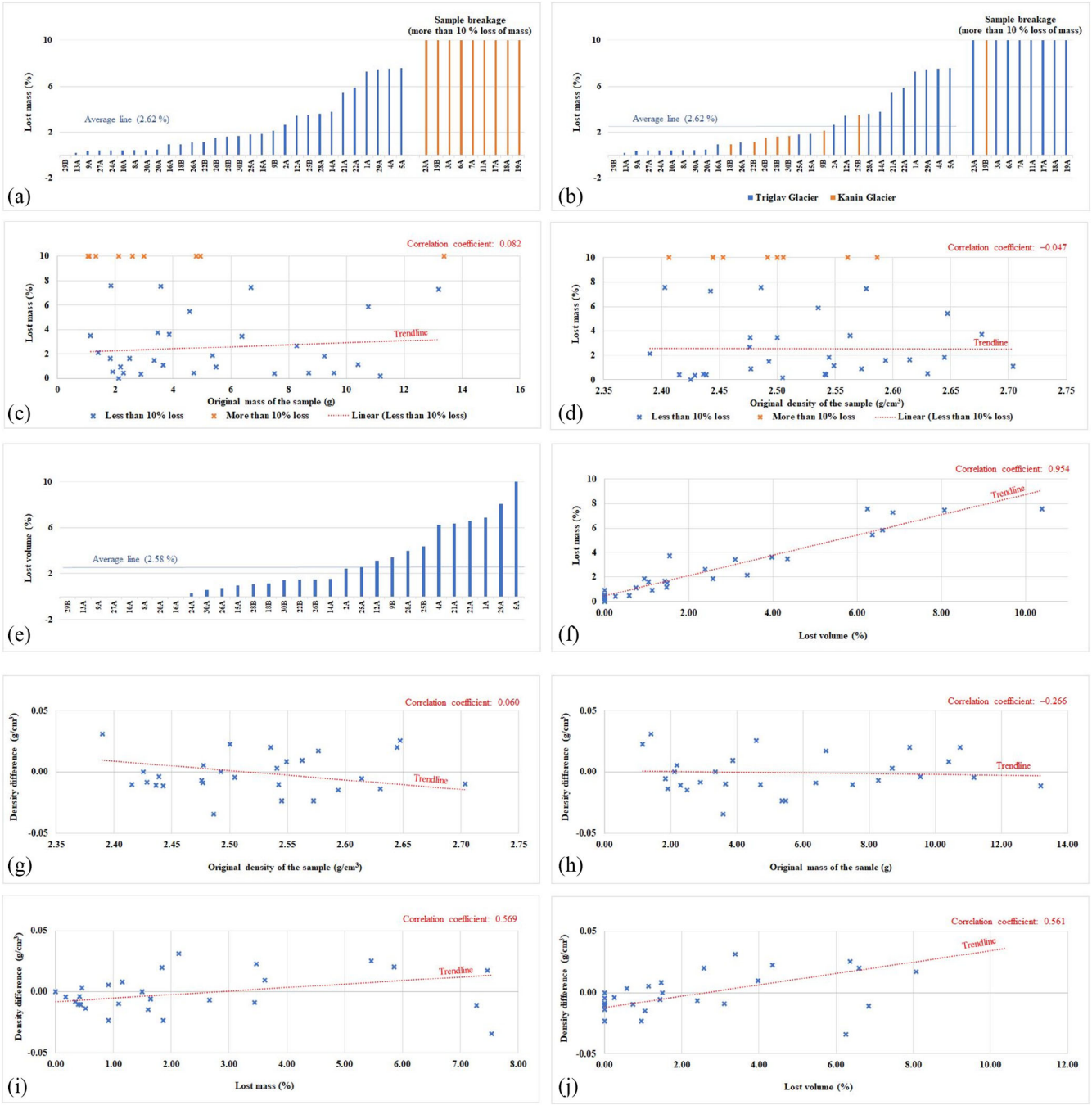

FIGURE 4 Columnar and correlation scatter charts. (a) The percentage of loss mass including the samples that experienced more than 10 % of loss mass due to breakage (see the same colour division in (c) and (d). (b) The percentage of loss mass illustrating Triglav and Kanin glaciers. (c) The percentage of loss mass in correlation to the original mass of the samples. (d) The percentage of loss mass in correlation to the percentage of loss volume. (e) The percentage of loss volume (for samples that experienced less than 10 % of loss mass). (f) The percentage of loss mass in correlation to the percentage of loss volume. (g) The density difference in correlation to the original density of the samples. (h) The density difference in correlation to the original mass of the samples. (i) The density difference in correlation to the percentage of loss mass. (j) The density difference in correlation to the percentage of loss volume.

The correlation coefficient between the absolute density difference and the original density is 0.060, indicating an extremely weak positive relationship (Figure 4g). This suggests that the magnitude of density changes (irrespective of being positive or negative) is not significantly influenced by the original density of the samples. Eleven samples experienced positive changes in density, with a mean increase of 0.0217 g/cm^3. Eighteen samples experienced negative changes in density, with a mean decrease of −0.0144 g/cm^3. The prevalence of negative changes (larger count) suggests that density reductions are more common than increases. However, the difference in magnitudes (mean absolute changes) is relatively small, indicating that both types of changes occur but may not statistically favour one over the other.

The correlation coefficient between the absolute density difference (the magnitude of change, irrespective of direction) and the original mass is −0.266 (Figure 4h). This indicates a weak negative relationship, suggesting that larger samples tend to experience slightly smaller absolute changes in density after frost weathering.

The correlation coefficient between the percentage of mass loss and absolute density difference is 0.569 (Figure 4i), indicating a

moderate positive relationship. This suggests that greater mass loss percentages tend to coincide with larger absolute changes in density. In addition, the correlation coefficient between the percentage of loss of apparent volume and absolute density difference is 0.561 (Figure 4j), also indicating a moderate positive relationship. This suggests that greater apparent volume loss percentages are associated with larger absolute density changes. Both correlations reveal that as the sample undergoes greater physical changes (mass or volume loss), it experiences correspondingly greater alterations in density, irrespective of the direction of the density change (increase or decrease).

3.4 | Freeze–thaw cycles from the Kredarica Meteorological Station

Table 3 provides the calculated freeze–thaw cycles based on the data from the Kredarica Meteorological Station, which is located in proximity to the Triglav Glacier (Figure 2f). It offers a comprehensive view of how different freeze–thaw scenarios (determined by temperature thresholds and snow cover conditions) affect the frequency of transitions and cycles. The results show that when all transitions at 0°C are included, regardless of snow cover (Scenario 1), the number of cycles is highest, averaging 44.82 per year. Excluding the zero-degree threshold (Scenario 2) results in a slightly reduced annual cycle rate of 42.27, while further limiting the threshold to below −3°C (Scenario 3) reduces the annual cycles by more than half to 19.49. These patterns indicate that the choice of freezing threshold significantly affects the calculated cycle frequency, with stricter temperature thresholds (e.g., <−3°C) greatly reducing the estimated freeze–thaw activity.

Snow cover is another critical factor influencing the calculated cycles. For instance, when snow cover is limited to less than 40 cm, the number of cycles per year decreases across all temperature thresholds compared to scenarios with no snow cover limitations. Scenario 4, which accounts for snow cover under 40 cm and transitions at 0°C, shows an average of 17.7 cycles per year, whereas Scenario 7, which excludes snow cover entirely, reduces the frequency to 9.85 cycles annually.

4 | DISCUSSION

The presence of breakage within 23% of the samples and the average mass loss of 2.62% for the remaining samples where the mass loss due to shredding did not exceed 10% indicate the susceptibility of subglacial carbonates to frost weathering. The data shows both mass reduction and outright breakage, indicating that frost weathering (Prick, 2004b) has varying impacts on subglacial carbonates, from surface-level weathering to complete structural failure. The observed non-linear decay patterns align with previous studies (e.g., Martínez-Martínez et al., 2013), which describe weathering processes where progressive damage culminates in rapid fragmentation. For example, samples with an average density of 2.50 g/cm^3 exhibited similar tendencies, with those closer to 2.40 g/cm^3 showing marginally higher susceptibility to breakage, indicating that porosity may play a role in localised structural vulnerabilities as discussed in Knopp et al. (2022).

The weak correlations between original mass or density and the percentage of mass loss emphasise the complex interplay of factors influencing weathering. While larger masses logically require more cycles to degrade to sand-sized particles, the data demonstrate that initial mass alone does not significantly govern weathering rates. This weak correlation, coupled with the observed heterogeneity in outcomes among samples with comparable properties, underscores the multifactorial nature of freeze–thaw weathering. Characteristics which have an effect on frost durability of the rock such as microstructure, pore geometry, laminations and pre-existing fractures (Chen et al., 2021; Deprez et al., 2020; Lai et al., 2024; Nicholson & Nicholson, 2000; Qiu, Fan, & Du, 2024; Rusin & Świercz, 2017; Rusin, Świercz, & Owsiak, 2015) likely interact to modulate the observed variability. For instance, while a sample with a high initial mass of 13.19 g showed less than 5% mass loss, another smaller sample weighing 2.89 g exhibited similar resistance, challenging simplistic assumptions about size and durability.

In the context of density changes, the study found that 11 samples experienced positive changes in density, while 18 exhibited negative changes, with a mean absolute difference of 0.0217 g/cm^3 and −0.0144 g/cm^3, respectively. These changes, though small in magnitude, reveal that frost weathering can cause both compaction and loosening within the same material group (Qi et al., 2023a). The prevalence of negative density changes suggests that structural weakening dominates over compaction in most cases, likely due to the formation of microcracks and pore expansion (Deprez et al., 2020). Nevertheless, the differences in density changes were statistically minor, indicating that both types of outcomes are feasible, though not dominant in determining the overall weathering response.

Field observations from the Kanin and Triglav glaciers corroborate laboratory results, showing that subglacial carbonate crusts tend to

TABLE 3 Calculated number of freeze–thaw cycles for the Kredarica Meteorological Station.

Scenarios	Scenario type	Transitions (1955–2021)	Cycles (1955–2021)	Transitions per year	Cycles per year
Scenario 1	>0 °C| ≤ 0°C| > 0°C, snow cover	6,008	3,003	89.67	44.82
Scenario 2	>0 °C| < 0°C| > 0°C, snow cover	5,666	2,832	84.57	42.27
Scenario 3	>0 °C| < −3°C| > 0°C, snow cover	2,614	1,306	39.01	19.49
Scenario 4	>0 °C| ≤ 0°C| > 0°C, snow cover less than 40 cm	2,373	1,186	35.42	17.7
Scenario 5	>0 °C| < 0°C| > 0°C, snow cover less than 40 cm	2,207	1,103	32.94	16.46
Scenario 6	>0 °C| < −3°C| > 0°C, snow cover less than 40 cm	799	399	11.93	5.96
Scenario 7	>0 °C| ≤ 0°C| > 0°C, no snow cover	1,321	660	19.72	9.85
Scenario 8	>0 °C| < 0°C| > 0°C, no snow cover	1,223	611	18.25	9.12
Scenario 9	>0 °C| < −3°C| > 0°C, no snow cover	297	148	4.43	2.21

break into smaller fragments under natural freeze–thaw conditions (Figure 5). A total of 75% of laboratory samples with crusts experienced subglacial carbonate detachment of 2–5% after 56 cycles, a trend similarly observed in situ where detachment and fragmentation occur on subglacial carbonate patches. Similar detachments were for example reported between quartz and laminae of muscovite (Lubera, Krzemień, & Krzaklewski, 2022), or on limestone where breakup involved loosening and detachment of the upper layers of rock also along partings, bedding planes or shale interbeds (Dredge, 2018). This consistency between controlled experiments and natural observations lends credibility to the laboratory's predictive validity for subglacial weathering processes.

The variability in the shape, thickness and mass of our tested samples mirrors the natural heterogeneity of subglacial carbonates observed in situ. This diversity enhances the validity of the findings, ensuring that the results are not constrained to idealised, uniform samples, but rather extend to real-world applications where such uniformity is impossible to achieve due to natural processes (Church, 2011).

The data indicate that the variability in sample shape, thickness and mass has a limited direct correlation with the rate of weathering (Figure 4c,d). However, it needs to be noted that subglacial carbonates are "crusts" covering the bedrock. These crusts, especially when detached from the bedrock, have a profound flat shape, which is likely the additional reason for their susceptibility to frost weathering due to greater surface area and stress concentration due to disk-like geometry. While individual mass loss rates vary among samples, the differences in time required to reach sand-sized particles, when using a consistent percentage loss of 2.62%, the initial mass will influence weathering duration. Larger masses naturally require more cycles to achieve significant reduction; however, the correlation between initial mass and weathering outcomes is weak (Figure 4c). Similarly, density shows minimal correlation with mass and consequently also volume loss rates (Figure 4d,f), implying that material compactness or porosity, as measured, does not strongly govern weathering behaviour. Although geometric factors such as shape and thickness were not explicitly quantified, the variability in outcomes among samples with similar density or initial mass highlights the complex interplay of intrinsic material properties. The lack of strong correlations across measured parameters underscores the inherent heterogeneity of natural samples, reflecting the multifactorial nature of frost weathering (Zhao et al., 2024) and its dependence on diverse characteristics. This variability supports the value of using non-uniform samples to replicate realistic conditions and to capture the range of natural responses to freeze–thaw processes, which poses a constant discussion between laboratory-based and realistic implications of weathering (Matsuoka, 2001; Trudgill & Viles, 1998).

Field observations at freshly exposed subglacial carbonates at the edge of the retreating ice masses of the Kanin and Triglav glaciers showed that the size of samples within our laboratory study is representative of the field. Nevertheless, in places, subglacial carbonates cover the bedrock to a greater extent (i.e., patches of up to 0.5 m in diameter), which, theoretically, would represent a relatively heavy piece of a subglacial carbonate sample if removed from the bedrock in

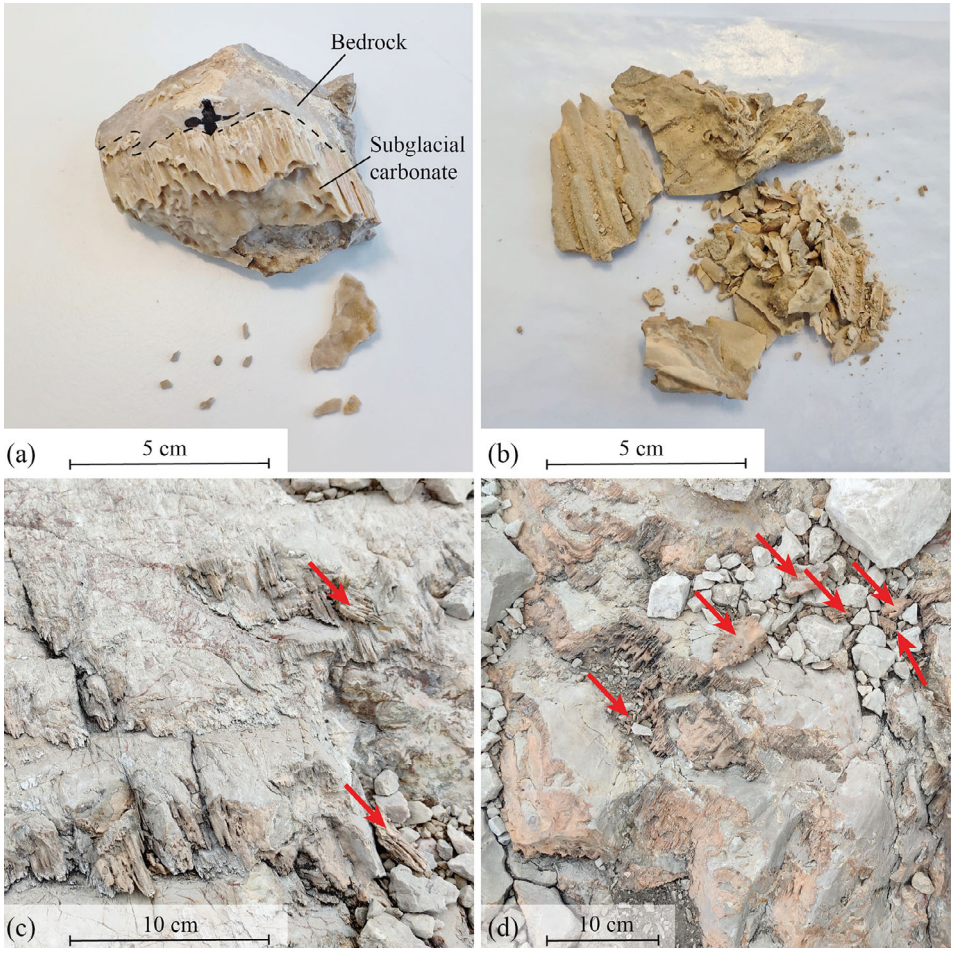

FIGURE 5 Breaking off of subglacial carbonates from the bedrock as evident from sample 31A after freeze–thaw procedure in a freezing tank (a) and as seen on the field (c and d). A complete breakage of the sample 6A (b).

one piece. Yet this is unlikely to happen as carbonate crust tends to break from the rock in smaller pieces, similar to our laboratory test of the limestone samples with attached subglacial carbonates. These samples experienced breakage of around 2–5% of subglacial carbonate crust after 56 freeze–thaw cycles; similar breakage is evident on the field (Figure 5c,d).

In addition, the variability observed within a single location for subglacial carbonates, such as differences in crystal size, morphology and isotopic composition, reflects localised conditions like meltwater availability and ice pressure rather than fundamental differences in formation processes. Sharp, Tison, & Fierens (1990) noted that even at a single site, subglacial carbonates maintain consistent origins tied to ice regelation, despite exhibiting minor compositional and structural differences. Across different locations, while variations in bedrock composition and hydrological dynamics influence specific deposit characteristics, the underlying process of formation through regelation remains uniform. This shared genesis suggests that subglacial carbonates, regardless of spatial variability, are fundamentally similar, providing a consistent signature of their subglacial origin.

The scalability and transferability of the results to other sites involve significant complexities, particularly in terms of the dimensional and temporal extrapolation of the findings (Schumm, 1979). While the study provides insights into the weathering of subglacial carbonates under freeze–thaw cycles, the question of original subglacial carbonate thickness remains a critical but unresolved variable if extrapolation of weathering time in the past is needed.

Nevertheless, an indicative observation of initial thickness may be observed near retreating glaciers (Figure 6a). In these locations, the visual absence of inner lamination in the subglacial carbonates suggests that they are of primary thickness, unaffected yet by weathering. Conversely, subglacial carbonates found further from glaciers often display exposed laminations (Figure 6b), indicating the removal of their uppermost layers through post-depositional weathering processes. The analogy to weathered and unweathered cave stalagmites provides a useful comparative framework (Figure 6c,d). Freshly exposed carbonates therefore provide a direct analogue for the primary subglacial carbonate state studied in the laboratory, while weathered deposits further from glaciers may no longer reflect their original form.

4.1 | Timely extrapolation

While it is tempting to provide the exact timeline of how quickly subglacial carbonates may weather to sand-sized particles in certain regions, there are a number of factors which raise uncertainties. Here, we discuss the complexity of such timely extrapolation and give examples from the Triglav Glacier area, which return a variety of possibilities.

4.1.1 | The number of freeze–thaw cycles

Firstly, we need to consider what rate of weathering the rocks might experience after 56 freeze–thaw cycles. Based on our data, 23% of the samples experienced breakage after 56 cycles. If we assume the conditions causing breakage continue similarly, this rate could suggest a similar proportion of breakage for subsequent cycles, assuming no saturation effects (e.g., no material limit to breaking apart further). The remaining 77% of the samples did not experience breakage but underwent mass loss and density changes. These samples might be at risk of entering the "breakage threshold" during additional cycles, especially if existing fractures or porosities are exacerbated.

We can assume three potential scenarios after additional freeze–thaw cycles:

Scenario A1: Linear progression in breakage rate: If material vulnerability progresses linearly, another 56 cycles might lead to an additional ~23% of samples experiencing breakage. This assumes that each set of 56 cycles has an equal capacity to induce breakage in previously unbroken samples. For example, assuming the same rate of breakage (23%) applies to the remaining samples, an additional seven samples (approximately 17% of the total) could experience breakage. This would result in a cumulative total of ~16 samples breaking after 112 cycles, representing about 41% of the total sample set.

FIGURE 6 Recently exposed subglacial carbonate near the Triglav Glacier (a) and subglacial carbonate approximately 150 m away (b), already showing internal lamination due to weathered upper part. Similar difference is observable between unweathered stalagmites (c) and weathered stalagmites (d).

Scenario A2: Accelerated breakage rate: Over successive cycles, microfractures and internal stresses might accumulate in surviving samples, making them increasingly prone to breakage. This could lead to a higher percentage of samples breaking during the next 56 cycles, potentially exceeding the observed 23% rate. For example, if the rate of breakage increases by 50% due to cumulative damage, an additional ~10 samples (approximately 26% of the total) might experience breakage. This would result in a cumulative total of ~19 samples breaking after 112 cycles, representing about 50% of the total sample set.

Scenario A3: Stabilisation in breakage rate: Some materials might resist further degradation due to inherent properties (e.g., low porosity or high crystallinity). If such samples represent a significant proportion of the dataset, the rate of new breakages could decrease over time. Here, we then need to consider the rate of the mass lost, calculated from the samples that experienced less than 10% of mass loss during the first 56 cycles. We can calculate the number of cycles required for each sample to reach sand-sized particles (2 mm diameter of a spherical grain equals ~4.19 mm^3, which in turn would be equivalent to ~0.011 g of calcite (assuming there is no porosity) (Robie & Bethke, 1962) based on the average weathering rate of 2.62% per 56 cycles, which gives an average of 12,670 cycles (ranging from 9,856 to 15,008). Alternatively, we can calculate the number of cycles required for each sample to reach sand-sized particles based on their individual mass loss rate percentage, which gives an average of 37,694 cycles, but a much more diverse range (ranging from 3,696 to 216,384).

4.1.2 | Freeze–thaw cycles versus years

For transparency, we provided nine different scenarios of how many freeze–thaw cycles a region near Triglav Glacier experiences in a year (Table 2). The insulating effect of snow cover leads to a decoupling of air and ground surface temperatures (Zhang, 2005), rendering Scenarios 1, 2 and 3 unsuitable for accurately calculating frost weathering rates. This decoupling arises because snow acts as a thermal buffer, significantly reducing the fluctuations in ground temperature that are critical for freeze–thaw cycles. The insulating effect is maximised when snow cover reaches an optimal thickness of approximately 40 cm (Zhang, 2005). This highlights the complexity of snow's impact on ground thermal regimes. Snow cover influences ground temperatures not just through its thickness but also through its timing, duration and melt-refreeze dynamics, including the latent heat associated with these processes (Zhang, 2005). Therefore, scenarios assuming a complete absence of snow cover (Scenarios 7, 8 and 9) are overly conservative and unrealistic, given that snow cover persists across much of the year in the study area (in the area of the Triglav Glacier about 260 days per year) (Hrvatin & Zorn, 2020). The most realistic scenarios are likely to be those involving partial snow cover, such as Scenarios 4, 5 and 6.

Under natural conditions, the freezing point of pure water is 0°C, but in porous materials or in the presence of solutes, the freezing point is depressed below 0°C (Kozlowski, 2009). This eliminates Scenarios 1, 4 and 7, as they assume freezing events at exactly 0°C. Additionally, ice segregation – a dominant mechanism of frost weathering – occurs primarily at temperatures below 0°C, often at lower thresholds around −3°C or below (Hales & Roering, 2005; Hallet, 2006; Murton, Peterson, & Ozouf, 2006). Although the specific type of frost weathering was not monitored in this study, the experimental freezing tank reached temperatures as low as −10°C. Based on these considerations, the most realistic scenarios for frost weathering in this study are Scenarios 3, 6 and 9, with Scenario 6 as the most likely when factoring in both temperature thresholds and the presence of snow cover.

Scenario 6, which incorporates transitions below −3°C and assumes snow cover under 40 cm, is the most representative for frost weathering rate calculations. This scenario predicts an average of 5.96 effective freeze–thaw cycles per year. Such a rate is plausible given the rugged alpine topography and the variable but often incomplete snow cover around the Triglav Glacier. The thermal inertia of thicker rock profiles, which might delay temperature shifts, is unlikely to play a significant role here, as supported by Anderson (1998). Furthermore, the lack of protective regolith ensures that subglacial carbonates are directly exposed to freeze–thaw stresses, increasing their susceptibility to weathering.

Nevertheless, it is important to acknowledge the variability in seasonal snow cover, which fluctuates widely both spatially and temporally across the complex alpine terrain of the Triglav Glacier. These fluctuations introduce additional uncertainty into freeze–thaw cycle calculations, as local variations in snow depth and the timing could either amplify or diminish the impact of frost weathering processes. While Scenario 6 provides a reasonable estimate for weathering rates under current conditions, ongoing changes in climate and snow cover patterns (Hrvatin & Zorn, 2020) may shift the balance of influencing factors, potentially altering the dominant weathering regimes in the future.

Using Scenario 6, the results suggest that the 56 measured cycles in the laboratory are equivalent to frost weathering over a period of 9.4 years. However, before this degradation to sand-sized particles, the initial detachment of subglacial carbonate from the bedrock must occur. Laboratory results indicate that 75% of the subglacial carbonate crusts experienced detaching after 56 freeze–thaw cycles, albeit incrementally, with 2–5% detachment occurring per cycle batch. This detachment is a critical precursor to subsequent frost-weathering processes. Given the high variability in sample responses, the initial detachment process itself introduces significant uncertainty to the overall weathering timeline. For example, if every 56 cycles a shred that represents 2% of the initial amount of subglacial carbonate crust would break off, then roughly 2,800 cycles would be needed for a complete detachment, corresponding to ~500 years. Roughly 1,120 cycles (~200 years) would be needed if 5% would be detached each time.

The further potential progression of weathering and breakage should be considered through three scenarios discussed in Section 4.1.1. Based on Scenario A1, which assumes a linear progression in the breakage rate, approximately 41% of the total samples would break after 112 cycles which corresponds to ~20 years. However, real-world environmental systems are rather characterised by nonlinear complexity (Phillips, 2003). In Scenario A2, the breakage rate accelerates over successive cycles due to cumulative damage, leading to a higher percentage of samples breaking with each additional cycle batch. Here, 50% of the total sample breaking is expected after 112 cycles (~20 years). This scenario seems most realistic as the increasing number of freeze–thaw cycles raises the risk of fatigue

failure (Deprez et al., 2020; Matsuoka, 2001). Conversely, Scenario A3 proposes stabilisation in the breakage rate, where a subset of materials resists further fragmentation. Under this scenario, for example, the remaining samples would continue to weather in an average of 12,670 cycles (9,856–15,008 cycles) corresponding to ~2,100 years (~1,600 – ~2,500 years).

The progression of frost weathering is complex, and natural conditions introduce additional variability. Breakage, as observed in 23% of the samples after 56 cycles, is likely to propagate in phases over time, influenced by microstructural flaws and the cumulative impact of freeze–thaw stresses (Chen et al., 2021; Deprez et al., 2020; Ju et al., 2024; Qiu, Fan, & Du, 2024). As breakage occurs, the surface area of fragments increases, potentially accelerating subsequent mass loss through exposure to water ingress and freeze–thaw action. On the other hand, as the more vulnerable material is removed, the remaining fragments may exhibit slower weathering rates due to their increased resistance, which is partially analogue to the rock weathering processes slowing down in time (Colman, 1981). These dynamics suggest that weathering rates are unlikely to follow a strictly linear or exponential model but may instead fluctuate over time, as previously noted in studies of rock decay processes (Colman, 2017; Eppes et al., 2020).

4.2 | Additional weathering processes

This paper provides laboratory tests of the susceptibility of the subglacial carbonates to frost weathering, yet this Earth process rarely acts alone. Carbonate rock decay in cold environments is characterised by the combination of physical and chemical weathering processes (Prick, 2004b), comprising processes of frost action, hydration, thermal fatigue, pressure realise and chemical, salt or biologically-induced weathering (Hall, 1999; Hall & Thorn, 2011).

For example, carbonate surfaces (such as those of subglacial carbonates) are also exposed to chemical denudation, whose rates can vary between 0.009 and 0.14 mm/year in Alpine settings (Gabrovšek, 2009), implying that in 1,000 years the surface lowering by chemical denudation would be between 9 mm to 140 mm. This suggests that the exposed and on average 5 mm thick subglacial carbonates would have been denuded at this time even if the frost weathering had been ineffective.

In addition, sediment production in the southeastern Alps is high (Mikoš, Fazarinc, & Ribičič, 2006) as well as the kinetic energy of falling debris (Duffy, 2019), and subglacial carbonates are subjected also to the erosional processes of falling/bouncing/rolling debris down the slope, aiding to their overall quick weathering timeframe. This would especially affect the primary breakage of the subglacial carbonate from the host rock.

The susceptibility of the subglacial carbonates to frost weathering, chemical denudation and erosion processes of rock debris characterises them as features prone to rapid weathering. This indicates that the occurrence of subglacial carbonates strongly suggests a recent past of a glacial presence above them. The preservation of subglacial carbonates dated to periods such as the Younger Dryas and the Last Glacial Maximum, as reported by Lipar et al. (2021), is largely due to the protection provided by the constant presence of ice. This, in turn, could expose subglacial carbonates to a possible glacier abrasion, but since subglacial carbonates form in the lee positions of bedrock protuberances, it is likely that abrasion decreases as rock fragments diverge from the bed at sites of subglacial precipitation due to regelation ice growth (Lipar et al., 2021). In addition, as demonstrated by Steinemann et al. (2020), glacial abrasion on carbonate bedrock is minimal compared to crystalline bedrock, which promotes the preservation of subglacial carbonates on limestone plateaus in the Alps whilst underneath the ice cover.

5 | CONCLUSION

This study provides new insights into the susceptibility of subglacial carbonates to frost weathering by subjecting 39 subglacial carbonate samples to 56 freeze–thaw cycles under controlled laboratory conditions. The results reveal a significant susceptibility to weathering, with 23% of the samples experiencing breakage into shreds and the remaining samples exhibiting an average mass loss of 2.62%. Additionally, the experiments showed variable density changes and mass-volume correlations during weathering, suggesting a multifactorial nature of frost-induced degradation that is not directly governed by the initial mass or density of the samples. This aligns with field observations of subglacial carbonate fragments near the retreating Triglav and Kanin glaciers, which confirm the rapid weathering of subglacial carbonates in recently deglaciated environments. In addition, while the controlled freeze–thaw cycles provide a quantitative estimate of weathering rates, subglacial carbonates are also subject to other weathering processes, including chemical denudation and physical impact from debris. These additional factors, absent in the laboratory setting, likely accelerate real-world weathering beyond the rates observed in controlled conditions.

Using data from the Kredarica Meteorological Station, the experimental freeze–thaw cycles were extrapolated to approximate natural weathering rates, indicating that the 56 laboratory cycles correspond to approximately 9.4 years of exposure. While this provides a useful framework for estimating long-term weathering timelines, the complexity of freeze–thaw dynamics, coupled with the insulating effects of snow cover and the variability in material properties, introduces significant uncertainty. Detachment of subglacial carbonates from the bedrock, observed in 75% of samples after 56 cycles, is an essential precursor to subsequent weathering, further complicating timely extrapolation. Despite these challenges, this study demonstrates the fragility of subglacial carbonates and their rapid breakdown under freeze–thaw conditions.

ACKNOWLEDGEMENTS

This research has been supported by the Slovenian Research and Innovation Agency (grant nos. J6-3141, P6-0101 and I0-0031). The rock samples in Triglav National Park were collected based on the permit No. 35619-6/2023-2.

CONFLICT OF INTEREST STATEMENT

The authors declare no competing interests.

ORCID

Matej Lipar https://orcid.org/0000-0003-4414-0147
Mateja Ferk https://orcid.org/0000-0003-0145-7590

REFERENCES

Aharon, P. (1988) Oxygen, carbon and U-series isotopes of aragonites from Vestfold Hills, Antarctica: clues to geochemical processes in subglacial environments. *Geochimica et Cosmochimica Acta*, 52(9), 2321–2331. Available from: https://doi.org/10.1016/0016-7037(88)90134-2

Anderson, R.S. (1998) Near-surface thermal profiles in Alpine bedrock: implications for the frost weathering of rock. *Arctic and Alpine Research*, 30(4), 362–372. Available from: https://doi.org/10.2307/1552008

Antonini, R., & Squassino, P. (1992). Fenomeni carsici di Planina Goricica. Alpine caves: alpine karst system and their environmental context(33-39).

Audra, P. (2000) Le karst haut alpin du Kanin (Alpes juliennes, Slovénie-Italie). *Karstologia*, 35(1), 27–38. Available from: https://doi.org/10.3406/karst.2000.2456

Benn, D.I. & Evans, D.J.A. (2010) *Glaciers & glaciation*, 2nd edition. London: Routledge 802 pp.

Chen, L., Li, K., Song, G., Zhang, D. & Liu, C. (2021) Effect of freeze-thaw cycle on physical and mechanical properties and damage characteristics of sandstone. *Scientific Reports*, 11(1), 12315. Available from: https://doi.org/10.1038/s41598-021-91842-8

Church, M. (2011) Observations and experiments. In: Gregory, K.J. & Goudie, A.S. (Eds.) *The SAGE handbook of geomorphology*. London, UK: SAGE Publications, pp. 121–141.

Colman, S.M. (1981) Rock-weathering rates as functions of time. *Quaternary Research*, 15(3), 250–264. Available from: https://doi.org/10.1016/0033-5894(81)90029-6

Colucci, R.R. (2016) Geomorphic influence on small glacier response to post-Little Ice Age climate warming: Julian Alps, Europe. *Earth Surface Processes and Landforms*, 41(9), 1227–1240. Available from: https://doi.org/10.1002/esp.3908

Colucci, R.R., Forte, E., Boccali, C., Dossi, M., Lanza, L., Pipan, M., et al. (2014) Evaluation of internal structure, volume and mass of glacial bodies by integrated LiDAR and ground penetrating radar surveys: the case study of Canin Eastern Glacieret (Julian Alps, Italy). *Surveys in Geophysics*, 36(2), 231–252. Available from: https://doi.org/10.1007/s10712-014-9311-1

Deprez, M., De Kock, T., De Schutter, G. & Cnudde, V. (2020) A review on freeze-thaw action and weathering of rocks. *Earth-Science Reviews*, 203, 103143. Available from: https://doi.org/10.1016/j.earscirev.2020.103143

Dredge, L.A. (2018) Breakup of limestone bedrock by frost shattering and chemical weathering, eastern Canadian Arctic. *Arctic and Alpine Research*, 24(4), 314–323. Available from: https://doi.org/10.1080/00040851.1992.12002963

Duffy, J.D. (2019) *Estimating rockfall kinetic energy as a function of rock mass, 70th highway geology symposium*. Portland, Oregon: The Oregon Department of Transportation, pp. 1–10.

Eppes, M.C., Magi, B., Scheff, J., Warren, K., Ching, S. & Feng, T. (2020) Warmer, wetter climates accelerate mechanical weathering in field data, independent of stress-loading. *Geophysical Research Letters*, 47(24), 1–11. Available from: https://doi.org/10.1029/2020GL089062

Ferk, M., Gabrovec, M., Komac, B., Zorn, M. & Stepišnik, U. (2017) Pleistocene glaciation in Mediterranean Slovenia. *Geological Society, London, Special Publications*, 433(1), 179–191. Available from: https://doi.org/10.1144/SP433.2

Ford, D.C., Fuller, P.G. & Drake, J.J. (1970) Calcite precipitates at the soles of temperate glaciers. *Nature*, 226(5244), 441–442. Available from: https://doi.org/10.1038/226441a0

Frisia, S., Weyrich, L.S., Hellstrom, J., Borsato, A., Golledge, N.R., Anesio, A.M., et al. (2017) The influence of Antarctic subglacial volcanism on the global iron cycle during the Last Glacial Maximum. *Nature Communications*, 8(1), 15425. Available from: https://doi.org/10.1038/ncomms15425

Gabrovec, M., Hrvatin, M., Komac, B., Ortar, J., Pavšek, M., Topole, M., Triglav Čekada, M., & Zorn, M. (2014) *Triglavski ledenik [Triglav Glacier]. Geografija Slovenije, 30*. Založba ZRC, Ljubljana, 252 pp, https://doi.org/10.3986/9789610503644

Gabrovšek, F. (2009) On concepts and methods for the estimation of dissolutional denudation rates in karst areas. *Geomorphology*, 106(1–2), 9–14. Available from: https://doi.org/10.1016/j.geomorph.2008.09.008

Hales, T.C. & Roering, J.J. (2005) Climate-controlled variations in scree production, Southern Alps. *New Zealand. Geology*, 33(9), 701. Available from: https://doi.org/10.1130/G21528.1

Hall, K. (1999) The role of thermal stress fatigue in the breakdown of rock in cold regions. *Geomorphology*, 31(1–4), 47–63. Available from: https://doi.org/10.1016/S0169-555X(99)00072-0

Hall, K. & Thorn, C. (2011) The historical legacy of spatial scales in freeze–thaw weathering: misrepresentation and resulting misdirection. *Geomorphology*, 130(1–2), 83–90. Available from: https://doi.org/10.1016/j.geomorph.2010.10.003

Hallet, B. (1976) Deposits formed by subglacial precipitation of CaCO3. *Geological Society of America Bulletin*, 87(7), 1003. Available from: https://doi.org/10.1130/0016-7606(1976)87<1003:DFBSPO>2.0.CO;2

Hallet, B. (2006) Why do freezing rocks break? *Science*, 314(5802), 1092–1093. Available from: https://doi.org/10.1126/science.1135200

Hart, J.K. & Boulton, G.S. (1991) The interrelation of glaciotectonic and glaciodepositional processes within the glacial environment. *Quaternary Science Reviews*, 10(4), 335–350. Available from: https://doi.org/10.1016/0277-3791(91)90035-S

Hellstrom, J., Augustinus, P., Fink, D., Drysdale, R. & Fabel, D. (2008) *U-Th-dated subglacial calcite preserves a record of basal meltwater discharge events of the East Antarctic ice sheet spanning the last 340,000 years, American Geophysical Union, Fall Meeting 2008*. San Francisco, California, USA: American Geophysical Union.

Higgins, J.A., Kurbatov, A.V., Spaulding, N.E., Brook, E., Introne, D.S., Chimiak, L.M., et al. (2015) Atmospheric composition 1 million years ago from blue ice in the Allan Hills, Antarctica. *Proceedings of the National Academy of Sciences of the United States of America*, 112(22), 6887–6891. Available from: https://doi.org/10.1073/pnas.1420232112

Hrvatin, M. & Zorn, M. (2020) Climate and hydrological changes in Slovenia's mountain regions between 1961 and 2018. *Economic- and Ecohistory*, 16(1), 201–218.

Ivy-Ochs, S., Kerschner, H., Reuther, A., Preusser, F., Heine, K., Maisch, M., et al. (2008) Chronology of the last glacial cycle in the European Alps. *Journal of Quaternary Science*, 23(6–7), 559–573. Available from: https://doi.org/10.1002/jqs.1202

Ju, X., Niu, F., Liu, M. & Luo, J. (2024) Evolution characteristics of freeze–thaw-induced sandstone damage under water immersion conditions in Changdu, Tibet, China. *Cold Regions Science and Technology*, 217, 104013. Available from: https://doi.org/10.1016/j.coldregions.2023.104013

Kerschner, H. & Ivy-Ochs, S. (2008) Palaeoclimate from glaciers: examples from the eastern Alps during the Alpine Lateglacial and early Holocene. *Global and Planetary Change*, 60(1–2), 58–71. Available from: https://doi.org/10.1016/j.gloplacha.2006.07.034

Knopp, J., Steger, H., Moormann, C. & Blum, P. (2022) Influence of weathering on pore size distribution of soft rocks. *Geotechnical and Geological Engineering*, 40(11), 5333–5346. Available from: https://doi.org/10.1007/s10706-022-02217-3

Kozlowski, T. (2009) Some factors affecting supercooling and the equilibrium freezing point in soil–water systems. *Cold Regions Science and Technology*, 59(1), 25–33. Available from: https://doi.org/10.1016/j.coldregions.2009.05.009

Kunaver, J. (1983) Geomorphology of the Kanin Mountains with special regard to the glaciokarst. *Geografski Zbornik*, 22, 197–346.

Lacelle, D. (2007) Environmental setting, (micro)morphologies and stable C–O isotope composition of cold climate carbonate precipitates—a review and evaluation of their potential as paleoclimatic proxies. *Quaternary Science Reviews*, 26(11–12), 1670–1689. Available from: https://doi.org/10.1016/j.quascirev.2007.03.011

Lai, R., Zhang, Z., Zhu, J., Xu, Z., Wei, X., Liu, X., et al. (2024) Deterioration mechanisms of tuff with surface fractures under freeze-thaw cycles. *Scientific Reports*, 14(1), 13402. Available from: https://doi.org/10.1038/s41598-024-62886-3

Lemmens, M., Lorrain, R. & Haren, J. (1982) Isotopic composition of ice and subglacially precipitated calcite in an Alpine area. *Zeitschrift für Gletscherkunde Und Glazialgeologie*, 18(2), 151–159.

Lipar, M., Lojen, S., Breg Valjavec, M., Andrič, M., Šmuc, A., Levanič, T., et al. (2024) Holocene climate variability in Slovenia: a review. *Acta Geographica Slovenica*, 64(2), 7–40. Available from: https://doi.org/10.3986/AGS.12798

Lipar, M., Martín-Pérez, A., Tičar, J., Pavšek, M., Gabrovec, M., Hrvatin, M., et al. (2021) Subglacial carbonate deposits as a potential proxy for a glacier's former presence. *The Cryosphere*, 15, 17–30.

Lubera, E., Krzemień, K. & Krzaklewski, P. (2022) Frost weathering of selected Tatra rocks in the light of laboratory tests. *Studia Geomorphologica Carpatho-Balcanica*, LVI-LVII, 5–29.

Martínez-Martínez, J., Benavente, D., Gomez-Heras, M., Marco-Castaño, L. & García-del-Cura, M.Á. (2013) Non-linear decay of building stones during freeze–thaw weathering processes. *Construction and Building Materials*, 38, 443–454. Available from: https://doi.org/10.1016/j.conbuildmat.2012.07.059

Matsuoka, N. (2001) Microgelivation versus macrogelivation: towards bridging the gap between laboratory and field frost weathering. *Permafrost and Periglacial Processes*, 12(3), 299–313. Available from: https://doi.org/10.1002/ppp.393

Mikoš, M., Fazarinc, R. & Ribičič, M. (2006) Sediment production and delivery from recent large landslides and earthquake-induced rock falls in the Upper Soča River Valley, Slovenia. *Engineering Geology*, 86(2–3), 198–210. Available from: https://doi.org/10.1016/j.enggeo.2006.02.015

Murton, J.B., Peterson, R. & Ozouf, J.C. (2006) Bedrock fracture by ice segregation in cold regions. *Science*, 314(5802), 1127–1129. Available from: https://doi.org/10.1126/science.1132127

Ng, F. & Hallet, B. (2002) Patterning mechanisms in subglacial carbonate dissolution and deposition. *Journal of Glaciology*, 48(162), 386–400. Available from: https://doi.org/10.3189/172756502781831214

Nicholson, D.T. & Nicholson, F.H. (2000) Physical deterioration of sedimentary rocks subjected to experimental freeze-thaw weathering. *Earth Surface Processes and Landforms*, 25(12), 1295–1307. Available from: https://doi.org/10.1002/1096-9837(200011)25:12<1295::AID-ESP138>3.0.CO;2-E

O'Brien, S.R., Mayewski, P.A., Meeker, L.D., Meese, D.A., Twickler, M.S. & Whitlow, S.I. (1995) Complexity of Holocene climate as reconstructed from a Greenland ice core. *Science*, 270(5244), 1962–1964. Available from: https://doi.org/10.1126/science.270.5244.1962

Ogrin, D., Repe, B., Štaut, L., Svetlin, D. & Ogrin, M. (2023) Podnebna tipizacija Slovenije po podatkih za obdobje 1991–2020. *Dela*, 59(1), 5–89.

Palacios, D., Hughes, P.D., García-Ruiz, J.M. & Andrés, N. (2022) *European glacial landscapes*. Amsterdam: Elsevier.

Park, J., Hyun, C.-U. & Park, H.-D. (2014) Changes in microstructure and physical properties of rocks caused by artificial freeze–thaw action. *Bulletin of Engineering Geology and the Environment*, 74(2), 555–565. Available from: https://doi.org/10.1007/s10064-014-0630-8

Peterson, J.A. & Moresby, J.F. (1979) Subglacial travertine and associated deposits in the Carstensz area, Irian Jaya, Republic of Indonesia. *Zeitschrift Fur Gletscherkunde Und Glazialgeologie*, 15(1), 23–29.

Phillips, J.D. (2003) Sources of nonlinearity and complexity in geomorphic systems. *Progress in Physical Geography: Earth and Environment*, 27(1), 1–23. Available from: https://doi.org/10.1191/0309133303pp340ra

Pleničar, M., Ogorelec, B. & Novak, M. (2009) *Geologija Slovenije [The geology of Slovenia]*. Ljubljana: Geološki zavod Slovenije 612 pp.

Prick, A. (2004a) Freeze-thaw cycle. In: Goudie, A.S. (Ed.) *Encyclopedia of geomorphology*, Vol. 1. London: Routledge, pp. 408–410.

Prick, A. (2004b) Frost and frost weathering. In: Goudie, A.S. (Ed.) *Encyclopedia of geomorphology*, Vol. 1. London: Routledge, pp. 412–415.

Qi, C., Guo, W., Li, Q. & Ma, X. (2023a) Decay function and damage strain model of fresh sandstone subjected to freeze–thaw cycles. *Bulletin of Engineering Geology and the Environment*, 82(5), 181. Available from: https://doi.org/10.1007/s10064-023-03193-5

Qi, C., Li, Q., Ma, X., & Guo, W. (2023b) Deterioration of fresh sandstone caused by experimental freeze-thaw weathering. *Cold Regions Science and Technology*, 214, 103956. https://doi.org/10.1016/j.coldregions.2023.103956

Qiu, B., Fan, L. & Du, X. (2024) Microstructure deterioration of sandstone under freeze-thaw cycles using CT technology: the effects of different water immersion conditions. *Journal of Rock Mechanics and Geotechnical Engineering*, 17(3), 1599–1611. Available from: https://doi.org/10.1016/j.jrmge.2024.02.002

Rabassa, J. (2010) El cambio climático global en la Patagonia desde el viaje de Charles Darwin hasta nuestros días. *Rev La Asoc Geológica Argentina*, 67, 139–156.

Rabassa, J. & Coronato, A. (2023) Subglacially precipitated carbonate deposits at Alvear Este and Martial Glaciers, Andes of Tierra del Fuego, Argentina. In: Cürebal, İ. & Poyraz, M. (Eds.) *IAG regional conference of geomorphology*. Cappadocia, Turkey: Turkish Society for Geomorphology, p. 120.

Ramovš, A. (2000) O Zlatenski plošči sensu Kossmat, 1913, Slatenskem pokrovu sensu Buser, 1986, Slatenskem narivu sensu Jurkovšek, 1987 in Triglavskem pokrovu sensu Ramovš, 1985 [About the Zlatna (Kossmat 1913), Slatna (Buser 1986; Jurkovšek 1987) or the Triglav Thrust (Ramovš 1985)]. *Geologija*, 43(1), 109–113. Available from: https://doi.org/10.5474/geologija.2000.010

Refsnider, K.A., Miller, G.H., Hillaire-Marcel, C., Fogel, M.L., Ghaleb, B. & Bowden, R. (2012) Subglacial carbonates constrain basal conditions and oxygen isotopic composition of the Laurentide ice sheet over Arctic Canada. *Geology*, 40(2), 135–138. Available from: https://doi.org/10.1130/G32335.1

Risheng, L., Jun, C., Gengnian, L. & Zhijiu, C. (2003) Characteristics of the subglacially-formed debris-rich chemical deposits and related subglacial processes of Qiangyong glacier, Tibet. *Journal of Geographical Sciences*, 13(4), 455–462. Available from: https://doi.org/10.1007/BF02837884

Robie, R.A. & Bethke, P.M. (1962) *Molar volumes and densities of minerals*. Reston, Virginia, USA: United States Department of the Interior; Geological Survey. Available from: https://doi.org/10.3133/70159012

Ruedrich, J., Kirchner, D. & Siegesmund, S. (2010) Physical weathering of building stones induced by freeze–thaw action: a laboratory long-term study. *Environmental Earth Sciences*, 63(7–8), 1573–1586. Available from: https://doi.org/10.1007/s12665-010-0826-6

Rusin, Z. & Świercz, P. (2017) Frost resistance of rock materials. *Construction and Building Materials*, 148, 704–714. Available from: https://doi.org/10.1016/j.conbuildmat.2017.04.198

Rusin, Z., Świercz, P. & Owsiak, Z. (2015) Effect of microstructure on frost durability of rock in the context of diagnostic needs. *Procedia Engineering*, 108, 177–184. Available from: https://doi.org/10.1016/j.proeng.2015.06.134

Schubert, H. (2002) *Handbuch der Mechanischen Verfahrenstechnik*. Wiley-VCH Verlag, Weinheim, https://doi.org/10.1002/3527603352

Schumm, S.A. (1979) Geomorphic thresholds: the concept and its applications. *Transactions of the Institute of British Geographers*, 4(4), 485. Available from: https://doi.org/10.2307/622211

Securo, A., Del Gobbo, C. & Colucci, R.R. (2022) Multi-year evolution of 75 snow and ice deposits in schachtdolines and shafts of recently deglaciated karst terrain: observations from Mount Canin-Kanin, Julian Alps, Europe. *Geomorphology*, 417, 1–13.

Securo, A., Forte, E., Martinucci, D., Pillon, S. & Colucci, R.R. (2022) Long-term mass-balance monitoring and evolution of ice in caves through structure from motion–multi-view stereo and ground-penetrating radar techniques. *Progress in Physical Geography: Earth and Environment*, 46(3), 422–440. Available from: https://doi.org/10.1177/03091333211065123

Sharp, M., Tison, J.-L. & Fierens, G. (1990) Geochemistry of subglacial calcites: implications for the hydrology of the basal water film. *Arctic and Alpine Research*, 22(2), 141–152. Available from: https://doi.org/10.1080/00040851.1990.12002776

Sharpe, D.R. & Shaw, J. (1989) Erosion of bedrock by subglacial meltwater, Cantley. *Quebec. Geological Society of America Bulletin*, 101(8), 1011–1020. Available from: https://doi.org/10.1130/0016-7606(1989)101<1011:EOBBSM>2.3.CO;2

Siman-Tov, S., Stock, G.M., Brodsky, E.E. & White, J.C. (2017) The coating layer of glacial polish. *Geology*, 45(11), 987–990. Available from: https://doi.org/10.1130/G39281.1

Slovenian Environment Agency. (2024) *Climate statistics for Kredarica Meteorological Station 1950–2020*. Slovenia: Slovenian Environment Agency.

Souchez, R.A. & Lemmens, M. (1985) Subglacial carbonate deposition: an isotopic study of a present-day case. *Palaeogeography, Palaeoclimatology, Palaeoecology*, 51(1–4), 357–364. Available from: https://doi.org/10.1016/0031-0182(85)90093-8

Steinemann, O., Ivy-Ochs, S., Grazioli, S., Luetscher, M., Fischer, U.H., Vockenhuber, C., et al. (2020) Quantifying glacial erosion on a limestone bed and the relevance for landscape development in the Alps. *Earth Surface Processes and Landforms*, 45(6), 1401–1417. Available from: https://doi.org/10.1002/esp.4812

Telbisz, T., Mari, L. & Szabó, L. (2011) Geomorphological characteristics of the Italian side of Canin Massif (Julian Alps) using digital terrain analysis and field observations. *Acta Carsologica*, 40(2), 255–266. Available from: https://doi.org/10.3986/ac.v40i2.10

Thomazo, C., Buoncristiani, J.-F., Vennin, E., Pellenard, P., Cocquerez, T., Mugnier, J.L., et al. (2017) Geochemical processes leading to the precipitation of subglacial carbonate crusts at Bossons Glacier, Mont Blanc Massif (French Alps). *Frontiers in Earth Science*, 5, 1–16. Available from: https://doi.org/10.3389/feart.2017.00070

Tičar, J., Lipar, M., Zorn, M. & Kozamernik, E. (2018) Triglavsko podzemlje [The underground world of Triglav Plateau]. In: Zorn, M., Mikša, P., Lačen Benedičič, I., Ogrin, M. & Kunstelj, A.M. (Eds.) *Triglav 240*. Ljubljana: Založba ZRC, pp. 131–145.

Tóth, G. & Veress, M. (2019) Examination of karren surfaces in the foreland of the glacier below Triglav. In: Veress, M., Telbisz, T., Tóth, G., Lóczy, D., Ruban, D.A. & Gutak, J.M. (Eds.) *Glaciokarsts*. Cham, Switzerland: Springer, pp. 339–347. Available from: https://doi.org/10.1007/978-3-319-97292-3

Triglav Čekada, M., Zorn, M. & Colucci, R.R. (2014) Changes in the area of the Canin (Italy) and Triglav glaciers (Slovenia) since 1893 based on archive images and aerial laser scanning. *Geodetski Vestnik*, 58(2), 274–313. Available from: https://doi.org/10.15292/geodetski-vestnik.2014.02.274-313

Trudgill, S.T. & Viles, H.A. (1998) Field and laboratory approaches to limestone weathering. *Quarterly Journal of Engineering Geology*, 31(4), 333–341. Available from: https://doi.org/10.1144/GSL.QJEG.1998.031.P4.06

White, W.A. (1970) Erosion of cirques. *The Journal of Geology*, 78(1), 123–126. Available from: https://doi.org/10.1086/627493

Widdowson, M. (1997) The geomorphological and geological importance of palaeosurfaces. *Geological Society, London, Special Publications*, 120(1), 1–12. Available from: https://doi.org/10.1144/GSL.SP.1997.120.01.01

Zhang, J.N., Yang, X., Chen, B., Wang, X., Hu, G., Tao, N., et al. (2023) Study of the freeze–thaw weathering's influence on thermal properties of stone artifacts. *Atmosphere*, 14(4), 666. Available from: https://doi.org/10.3390/atmos14040666

Zhang, T. (2005) Influence of the seasonal snow cover on the ground thermal regime: an overview. *Reviews of Geophysics*, 43(4), 1–23. Available from: https://doi.org/10.1029/2004RG000157

Zhao, Y., Hu, K., Han, D., Lang, Y. & Zhang, L. (2024) Multifactor-coupled study on freeze-thaw forces of rocks in cold regions. *Frontiers in Earth Science*, 12, 1–13. Available from: https://doi.org/10.3389/feart.2024.1404153

How to cite this article: Lipar, M., Zorn, M., Ferk, M., Cof, K. & Čretnik, J. (2025) The susceptibility of subglacial carbonates to frost weathering. *Earth Surface Processes and Landforms*, 50(5), e70055. Available from: https://doi.org/10.1002/esp.70055